Available online at www.sciencedirect.com
ScienceDirect
Materials Research Bulletin 43 (2008) 864–872
Materials Research Bulletin
www.elsevier.com/locate/matresbu

Visible-light-driven $NaTaO_{3-x}N_x$ catalyst prepared by a hydrothermal process

Hongbo Fu [a,b], Shicheng Zhang [b], Liwu Zhang [a], Yongfa Zhu [a,*]

[a] Department of Chemistry, Tsinghua University, Beijing 100084, PR China
[b] Department of Environment Science & Engineering, Fudan University, Shanghai 200433, PR China

Received 23 December 2006; accepted 3 May 2007
Available online 16 May 2007

Abstract

$NaTaO_{3-x}N_x$ catalyst has been successfully synthesized from N-doped Ta_2O_5 precursors by a simple hydrothermal process. The as-prepared samples were characterized by X-ray diffraction, X-ray photoelectron spectroscopy, and diffuse reflectance spectroscopy. Density functional theory calculations suggested that the valence band of the catalysts was composed of the hybrid O 2p and N 2p orbitals, and the visible-light sensitivity is due to the narrowing of the band gap by mixing N 2p and O 2p states. $NaTaO_{3-x}N_x$ catalyst could decompose the gaseous formaldehyde under the visible-light irradiation ($\lambda > 400$ nm), and its photocatalytic activity depended on N dopant concentration. $NaTaO_{2.943}N_{0.047}$ showed the highest photoactivity for the formaldehyde photodegradation.

Keywords: A. Oxides; B. Chemical synthesis; D. Catalytic properties; D. Semiconductivity

1. Introduction

Heterogeneous photocatalytic reactions at semiconductor surfaces represent a very active research field. Many oxide photocatalysts have been developed for energy problem and the increasingly stringent standards of environmental regulations. It has been reported that the perovskite-type alkali tantalates, $ATaO_3$ (A = Li, Na, and K) show reasonable activities for water splitting into H_2 and O_2 in a stoichiometric ratio under UV irradiation [1–3]. The layered structures avail for the separation of the reaction site for H_2 and O_2 evolution to avoid the back reaction. Among the catalysts examined to date, $NaTaO_3$ doped with La has demonstrated the highest quantum yield of water splitting, exceeding 50% when irradiated by UV light [1]. However, the valence band of $NaTaO_3$ predominantly consists of O 2p orbitals whose potential energy levels are located at a deep position of about 3 V versus NHE (or about −7.44 V versus vacuum level). Due to this fact, it is not active under visible-light irradiation [4].

Intense efforts are now being made to find catalysts that efficiently degrade pollutant or/and split water for hydrogen with visible-light. Substituting a cation or anion site in UV light sensitive photocatalysts by a foreign element is a general method for preparing visible-light sensitive photocatalysts. Recently, the band gap of TiO_2 has been narrowed successfully by doping with nonmetal cations, by replacing lattice oxygen with B, C, N, or S dopants [5–8]. It is widely recognized that the anionic nonmetal dopants, may be more appropriate for extension of photocatalytic activity into the visible-light region, because the related impurity states are supposed to be close to the

* Corresponding author. Tel.: +86 10 62783586; fax: +86 10 62787601.
E-mail address: zhuyf@mail.tsinghua.edu.cn (Y. Zhu).

0025-5408/$ – see front matter
doi:10.1016/j.materresbull.2007.05.013

valence band maximum. Furthermore, the position of the conduction band minimum, which must be kept at the level of the H_2/H_2O potential, when TiO_2 is used for the photoelectrolysis of water into hydrogen. Among all the nonmetal cations, substitutional N-doping was found to be particularly effective in decreasing the band gap of TiO_2 through the mixing of N 2p and O 2p states [9,10]. The presence of doped nitrogen extends the optical absorption of TiO_2 to the visible-light spectrum and enhances the visible-light-driven photocatalysis.

Although some of the knowledge accumulated on TiO_2 can be transferred to other catalysts, visible-light induced photoactivity due to N doping should be observed on the highly efficient catalyst itself to promote further development toward visible-light induced photocatalysis. However, to the best of our knowledge, N-doped $NaTaO_3$ is still not reported.

Traditionally, $NaTaO_3$ is produced from high temperature solid state reactions at above 1000 °C with the resulting aggregate requiring a subsequent milling process [11–13]. Problems associated with the preparation include incorporation of unreacted metal in the product, and lack of control over crystallinity and particle sizes, resulting in a decrease in the photocatalytic activity of a given catalyst to a great extent. Since excellent photocatalysts always requires homogeneous and pure powders with fine and uniform particle sizes, an alternative synthesis procedure is needed. The hydrothermal technique, which has widely been applied to the synthesis of nanosized photocatalysts is characterized by mild synthesis temperature, chemical homogeneity, high purity and controlled size and morphology which tends to improve or dramatically change the physical properties of the final products. The present authors have reported that the hydrothermal Bi_2WO_6 sample presented the enhanced photoactivity for the pollutants decomposition [14,15].

In the present study, $NaTaO_{3-x}N_x$ was first successfully prepared from the N-doped Ta_2O_5 precursor by a simple hydrothermal process. The optimum conditions of the preparation and photocatalytic reactions on N-doped $NaTaO_3$ were investigated to improve photocatalytic activities. The as-prepared samples were characterized by X-ray photoelectron spectroscopy (XPS), X-ray diffraction (XRD), UV–vis diffuse reflection spectroscopy (DRS). The formaldehyde (FAD) decomposition was used as a probe reaction to evaluate the photocatalytic properties of the catalyst. The relationship between the band structures and photocatalytic activities is also discussed.

2. Experimental

2.1. Preparation of the catalyst

Commercial Ta_2O_5 (99.99%) was treated in a flow reactor system in a N_2 gas atmosphere (1 atm) at 750 °C. Typical heating rates were 10 °C min^{-1}. For doping, N_2 flow was replaced by NH_3 for 0–60 min after the target temperature had been reached. Subsequently, polycrystalline powders were cooled in flowing N_2. The samples were the deep-red powders. $Ta_2O_{5-x}N_x$ and NaOH were chosen as starting materials for the hydrothermal synthesis of $NaTaO_{3-x}N_x$. In a typical synthesis procedure, 1.2 g NaOH and 0.442 g $Ta_2O_{5-x}N_x$ were added to 30 mL deionized water with magnetic stirring. A series of the reaction mixtures were sealed in a Teflon-lined stainless steel autoclave and heated in the temperature range of 60–200 °C under autogenous pressure for 12 h. After cooling, the product was filtered, washed and dried at ambient temperature.

All chemicals were analytical reagent grade quality and used without further purification. Deionized water was used throughout this study.

2.2. Characterization

XRD patterns of the powders were recorded at room temperature by a Bruker D8 advance X-ray diffractometer using the Cu Kα radiation and a 2θ scan rate of 2° min^{-1}. XPS analysis was measured on a PHI 5300 ESCA instrument using an Al Kα X-ray source at a power of 250 W. The pass energy of the analyzer was set at 35.75 eV and the base pressure of the analysis chamber was $<3 \times 10^{-9}$ Torr. The binding energy scale was calibrated with respect to the C1s peak of hydrocarbon contamination fixed at 285.0 eV. It was reported that the peak at around 400 eV corresponds to N 1s, derived from Ta–N bonds. However, because the peak area of N 1s was partly overlapped with that of Ta $4p_{3/2}$, a peak separation method was applied to calculate the peak area of N 1s. Therefore, the x values (nitrogen concentrations) were estimated by comparing the product of the 396 eV peak area multiplied by the nitrogen sensitive

factor to the product of the 531 eV peak area (O 1s, Ta–O bonds) multiplied by the oxygen sensitive factor [16]. UV–vis DRS was obtained using a Hitachi U-3010 spectrometer (Japan). $BaSO_4$ was the reference sample and the spectra were recorded in the range 200–700 nm.

2.3. Photocatalytic experiments

The photocatalytic activities of the samples were evaluated by the decomposition of FAD under the irradiation with visible-light ($\lambda > 400$ nm). A 500 W xenon lamp (the Institute of Electric Light Source, Beijing) was focused through a window, and a 400 nm cut-off filter was placed onto the window face of the cell to ensure the desired irradiation light. The average light intensity was 30 mW cm^{-2}. The radiant flux was measured with a power meter (the Institute of Electric Light Source, Beijing).

The catalysts were evenly and uniformly spread without open spaces in the sample over the irradiation area (approximately 9.4 cm^2) in 250 mL vessel. Irradiated light was absorbed only on the outer geometric surface of the powder. Certain concentration of the reactant gas was injected into the vessel and then the samples were stored in the dark. When the concentration of FAD was kept constant, the light irradiation started. The amounts of FAD were determined using a gas chromatograph (SP-502) with the FID detector.

3. Results and discussion

3.1. Structural characterization

Fig. 1 shows XRD patterns of the samples prepared from N-doped Ta_2O_5 precursor in NaOH solution (1 M) at the temperature scope of 60–200 °C. In the spectrum of the precursor, all the reflections can be readily indexed as the orthorhombic Ta_2O_5 (JPCDS 25-0922), and neither TaON nor Ta_3N_5 phases were observed [13]. Compared to XRD patterns of the precursor, ones of the sample prepared at 60 and 80 °C did not change. It is clearly seen that a partial crystallization of a perovskite-type $NaTaO_3$ has occurred during the hydrothermal treatment of the precursor at 100 °C for 12 h. A new peak at 10° appears, and the peak at 28° split into two peaks. The intensity of the peak at 32.5° became stronger greatly. With the temperature increase, the intensity the peak at 10° and two peaks at 28° decrease and disappear completely when the sample was prepared at 200 °C. The intensity of the peak at 32.5° enhanced clearly. A pure phase of $NaTaO_3$ was gained at 200 °C. All the reflections can be readily indexed as perovskite $NaTaO_3$ [space group: 10], identical to the reported data in the JCPDS card (74-2478), which is consistent with the data reported before [17].

To probe the effect of the N content on the crystal structure, Ta_2O_5 with the different N-doped content was selected as the precursors for $NaTaO_{3-x}N_x$ synthesis at 200 °C for 12 h. XRD patterns of the as-prepared samples are shown in

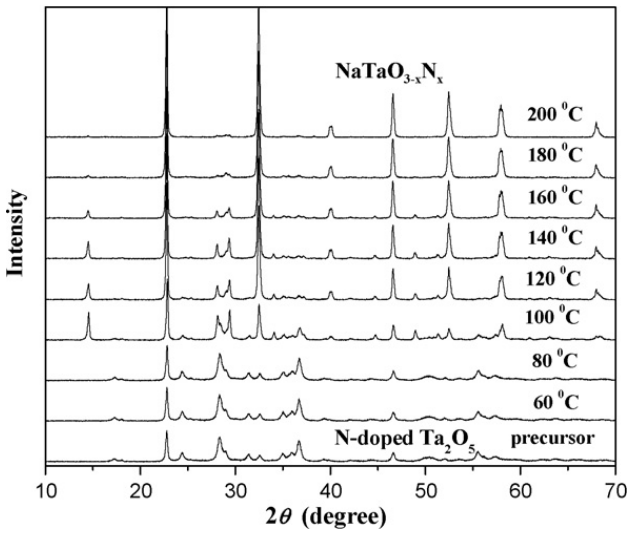

Fig. 1. XRD patterns of the samples prepared at different hydrothermal temperature for 12 h.

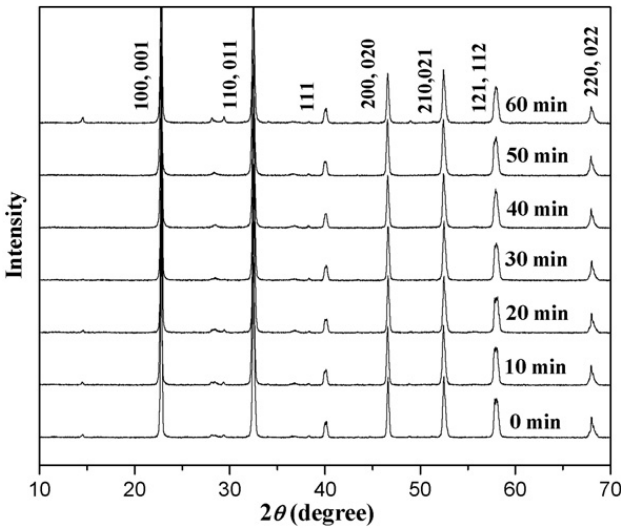

Fig. 2. XRD patterns of the samples prepared at 200 °C for 12 h from N-doped Ta_2O_5 with the different NH_3 annealing times.

Fig. 2. Replacing an O with an N atom in $NaTaO_3$ does not result in significant structural changes. This could be understood that the concentration of the doped N atom (given later) might be low to cause a shift, although it has a larger ion radius of 0.171 nm than that of O atom of 0.132 nm [13]. From HRTEM image of the sample (not shown), N doping do not change the morphology of $NaTaO_3$.

3.2. Optical properties

Fig. 3 shows DR spectra of the samples prepared from Ta_2O_5 precursors with the different N-doped contents at 200 °C. The as-prepared powders obviously absorbed visible-light. This absorption at 320–620 nm is related to the presence of nitrogen since it increases with nitrogen content [18]. Additionally, the absorption edge of new band well agrees with the reported value for the N-doped Ta_2O_5 system [18]. With the increase of N doping content, the absorption area in the visible region increased greatly. The band gap of the undoped $NaTaO_3$ was estimated to be 3.9 eV from the absorption edge. The absorption onsets of the doped samples have the slight red-shift with the increase of N doping content. These crystals are red in color, and the colors were darker gradually as x increase. Whereas, the undoped $NaTaO_3$ are colorless, yet clear. The presence of the visible absorption band indicates that nitrogen penetrates into the single crystal and effectively changes the electronic structure of the catalysts.

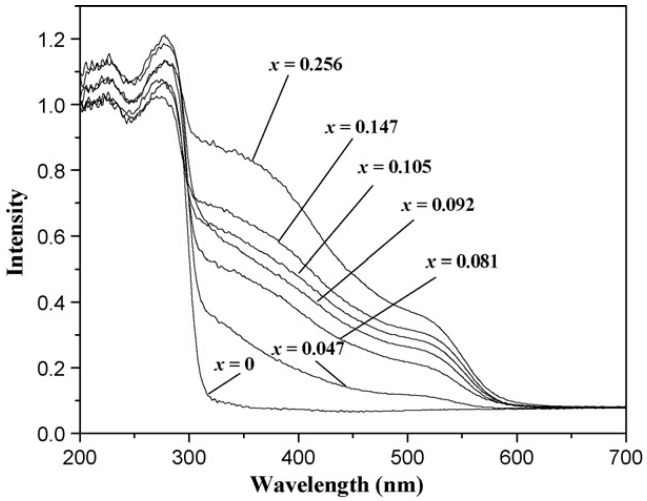

Fig. 3. DR spectra of $NaTaO_{3-x}N_x$ prepared from N-doped Ta_2O_5 with the different N doping content at 200 °C for 12 h.

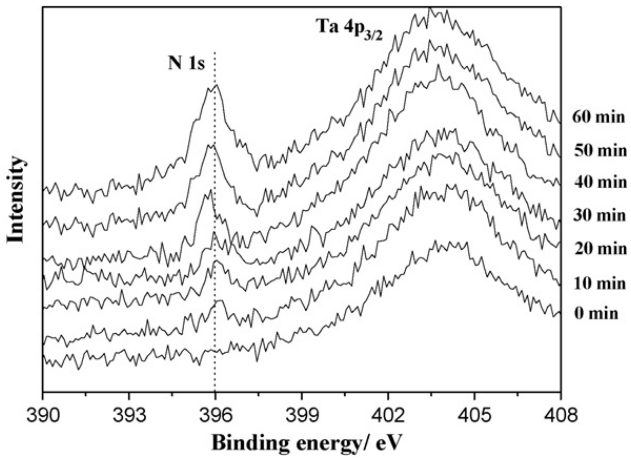

Fig. 4. N 1s peak around 400 eV regions in XPS of the samples prepared from N-doped Ta_2O_5 with the different NH_3 annealing times.

3.3. N content in the catalysts

Fig. 4 shows the N 1s spectra of the samples prepared at 200 °C for 12 h from N-doped Ta_2O_5 with the different NH_3 annealing times. A new peak at 396–397 eV was observed. This peak is generally considered as the evidence for the presence of Ta–N bonds, suggesting that the oxygen sites were substituted by nitrogen atoms [18]. Considering XRD patterns and XPS spectra, the powders were described as $NaTaO_{3-x}N_x$. As N-doped Ta_2O_5 with higher N doping content was selected as a precursor, the resulting product contained the higher N content, accordingly. The sample prepared from N_2 gas annealed precursor did not display a peak at 396 eV. The estimated x values from XPS spectra are listed in Table 1. With x value increase, the visible absorbance of the catalyst become stronger and the color become darker, which are in accordance with their absorbance spectra.

3.4. DFT electronic structure calculations

$NaTaO_3$ consist of corner-sharing TaO_6 octahedra with perovskite-like structure. The bond angle of Ta–O–Ta is 163°. The excited energy is delocalized in $NaTaO_3$ because its bond angle is close to 180 °C, resulting in high photoactivity for water splitting into H_2 when irradiated with UV light [17].

The quantum-mechanical calculations performed here are based on density functional theory (DFT) [19]. Exchange-correlation effects were taken into account by using the generalized gradient approximation (GGA) [20]. The total energy code CASTEP was used [21], which utilizes pseudopotentials to describe electron-ion interactions and represents electronic wavefunctions using a plane-wave basis set. The kinetic energy cut-off was set at 280 eV. The Brillouin-zone sampling was performed by using a k-grids of $3 \times 3 \times 3$ points for the calculations. We optimized the lattice parameters and atomic positions of $NaTaO_3$ by minimizing the total energy. The atomic positions of N-doped $NaTaO_3$ were optimized based on the theoretical lattice constants of $NaTaO_3$ without imposing any symmetry. N doping was modeled by replacing 1 oxygen atoms in the 35-atom supercell, as shown in Fig. 5. The resulting stoichiometry is $NaTaO_{3-x}N_x$ with $x = 0.0257$.

Table 1
x values in $NaTaO_{3-x}N_x$ catalysts prepared from N-doped Ta_2O_5 precursors with the different NH_3 annealing times

Annealing time (min)	x in $NaTaO_{3-x}N_x$
Air 60	0
NH_3 10	0.047
NH_3 20	0.081
NH_3 30	0.092
NH_3 40	0.105
NH_3 50	0.147
NH_3 60	0.256

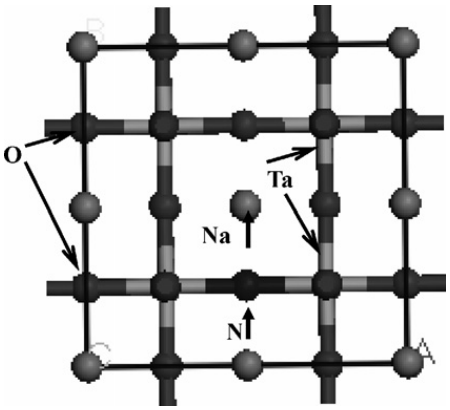

Fig. 5. Unit cells of N-doped $NaTaO_3$.

DFT result of $NaTaO_3$ is shown in Fig. 6(A). The occupied bands of $NaTaO_3$ were classified into four bands. The lower-energy side in the occupied bands consisted of solely Na 2s (1–8#). The middle part of the occupied bands consisted of Na 2p orbitals (9–32#) and O 2s + Ta 5s5p orbitals (33–55#), respectively. The higher-energy side, i.e., corresponded to the valence band (VB), consists of O 2p orbitals (56–126#). The bottom of conduction band (CB) was formed by Ta 5d orbitals, with a small contribution of O 2p orbitals (127–138#). Thus, the highest occupied and lowest unoccupied molecular orbital levels were composed of O 2p and Ta 5d orbitals, respectively. The band gap of TiO_2 was

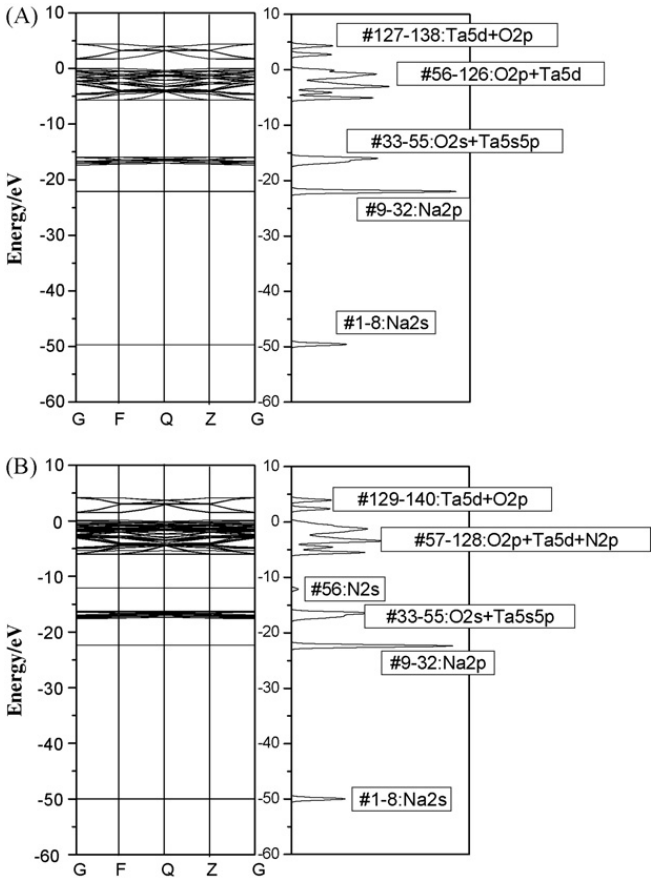

Fig. 6. Total DOS of $NaTaO_3$ (A) and $NaTaO_{3-x}N_x$ (B).

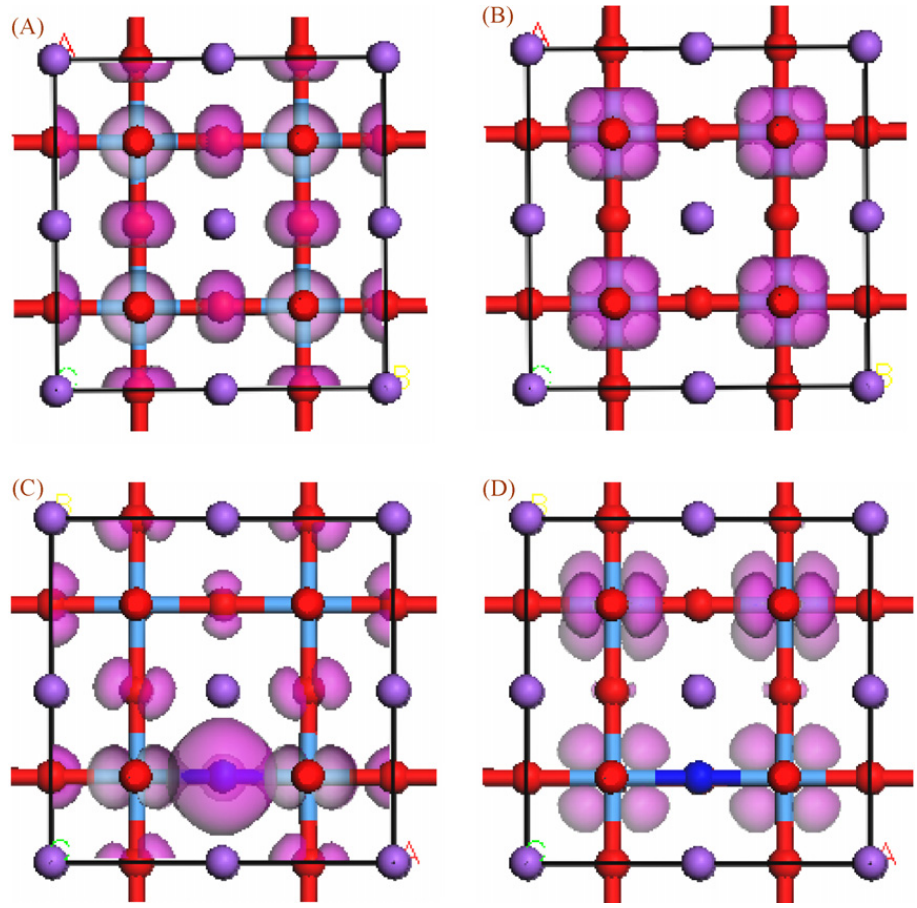

Fig. 7. Density contour maps of orbitals at the top of the valence band and bottom of the conduction band for $NaTaO_{3-x}N_x$: HOMO (A) and LUMO (B) before N doping; HOMO (C) and LUMO (D) after N doping.

estimated to be 1.71 eV. Generally, the band gap calculated by DFT is smaller than that obtained experimentally, which is frequently pointed out as a common feature of DFT calculations [22].

DFT result of N-doped $NaTaO_3$ is shown in Fig. 6(B). One can see that the VB of N-doped $NaTaO_3$ is composed of the hybrid orbitals of O 2p and N 2p. The calculated band gap of $NaTaO_3$ was narrowed by 0.21 eV due to N doping. Asahi et al. calculated by the band structure of $TiO_{2-x}N_x$, and reported that mixing N 2p and O 2p states narrowed the band gap [7]. The present DFT calculation of N-doped $NaTaO_3$ is in agreement with their conclusion.

Density contour maps of orbitals are shown in Fig. 7. The highest occupied molecular orbital (HOMO) of $NaTaO_3$ showed the p orbital lobes on O atom, indicated that the orbital was purely composed of O 2p orbitals. The lowest unoccupied molecular orbital (LUMO) was mainly formed by Ta 5d orbital. Both O 2p and N 2p orbitals are involved in HOMO of N-doped $NaTaO_3$. Thus, these results indicate that the higher part consists of the O 2p and N 2p orbitals in the valence band of N-doped $NaTaO_3$.

The result of electronic structure calculation showed that the valence band of $NaTaO_{3-x}N_x$ was composed of O 2p hybrid with N 2p, which enhanced the energy level of valance band, and resulted in a narrow band gap energy. Therefore, $NaTaO_{3-x}N_x$ can be driven under visible-light irradiation, and N is the candidate elements that are able to make the valence band higher.

3.5. Photocatalytic activity

To evaluate the photoactivity of the as-prepared samples, the gaseous FAD photodegradation over $NaTaO_{3-x}N_x$ was performed. The results are shown in Fig. 8. Irradiating the undoped $NaTaO_3$ ($x = 0$) with visible-light ($\lambda > 400$ nm) did not generate the decrease of FAD in concentration, as $NaTaO_3$ is not visible-light sensitive. The degradation of FAD, however, was observed from all the other samples. As the x value increased, the photoactivies of the samples decreased, which is similar with that in the case of N-doped TiO_2 or Ta_2O_5 [16,18]. $NaTaO_{2.943}N_{0.047}$ showed the

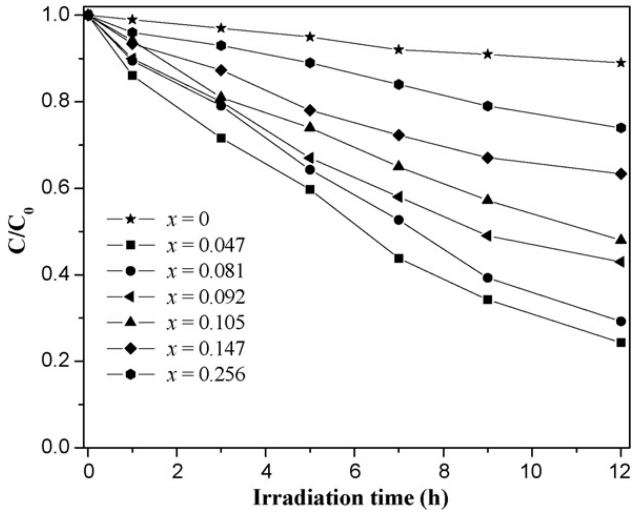

Fig. 8. The visible photoactivities of the as-prepared sample for the decomposition of FAD; $\lambda > 400$ nm; the initial concentration of FAD, 860 ppm.

highest activity for FAD decomposition. About 80% of FAD were photodegraded after 12 h in the presence of $NaTaO_{2.943}N_{0.047}$.

Lattice defects may act as recombination centers for photoinduced electrons and holes, thus reducing the net photocatalytic activity significantly [14,15]. The decrease in the photocatalytic activity of the sample with the increase of x values may therefore be understood in such a way, namely, that the abundant lattice defects acting as inactivation centers is increased due to more N doping, which could be observed from DR spectra and XPS results. It is well known that N doping act as a recombination center of photogenerated charge carriers, and thus deteriorate photocatalysis [18]. Therefore, the sample prepared at 200 °C showed the highest photoactivity due to the lower N-doped content.

As to the origin of visible-light responses for N-doped TiO_2, different mechanisms to date and no definite conclusion has been obtained yet. In the present study, DFT calculations indicate N-doping caused the narrowing of the band gap of the catalysts. Our results are in good agreement with the previous report about N-doped TiO_2 [18]. We concluded that the narrowing of the band gap by N doping is responsible for the visible-light response.

It is noted that visible-light induced activity of $NaTaO_{3-x}N_x$ catalyst for FAD photodegradation was relatively low. It may be considered that the doping of a foreign N element is disadvantageous to the photocatalysis judging from the following reasons: (i) N doping works as an electron-hole recombination center, (ii) the mobility of electrons or holes in the dopant level is small because the dopant forms not a band but a discrete level.

4. Conclusions

N-doped $NaTaO_3$ has prepared by a simple hydrothermal process. The as-prepared samples had nitrogen substituted at some of the oxygen sites in $NaTaO_3$. The valance band of $NaTaO_{3-x}N_x$ is composed of O 2p and N 2p orbitals and visible absorbance of the catalyst is inspired by the narrowing of the band due to N doping. The samples showed the photoactivities for the decomposition of the gaseous FAD under visible irradiation. The activity of the sample decreased with the increase of the N-doping concentration.

Acknowledgements

This work was partly supported by the Chinese National Science Foundation (20433010, 20571047) and Trans-Century Training Program Foundation for the Talents by the Ministry of Education, P.R. China, and China Postdoctoral Science Foundation (2005037050) for their financial support.

References

[1] H. Kato, K. Asakura, A. Kudo, J. Am. Chem. Soc. 125 (2003) 3082.
[2] T. Ishihara, H. Nishiguchi, K. Fukamachi, Y. Takita, J. Phys. Chem. B 103 (1999) 1.

[3] H. Kato, A. Kudo, Chem. Phys. Lett. 295 (1998) 487.
[4] G. Hitoki, T. Takata, J. Kondo, M. Hara, H. Kobayashi, K. Domen, Chem. Commun. (2002) 1698.
[5] W. Zhao, W. Ma, C. Chen, J. Zhao, Z. Shuai, J. Am. Chem. Soc. 126 (2004) 4782.
[6] S. Khan, M. Shahry, W.B. Ingler, Science 297 (2002) 2243.
[7] R. Asahi, T. Morikawa, T. Ohwaki, K. Aoki, Y. Taga, Science 293 (2001) 269.
[8] T. Ohno, T. Mitsui, M. Matsumura, Chem. Lett. 32 (2003) 364.
[9] H. Irie, Y. Watanabe, K. Hashimoto, J. Phys. Chem. B 107 (2003) 5483.
[10] X. Chen, C. Burda, J. Phys. Chem. B 108 (2004) 9867.
[11] Q. Zhang, L. Gao, Langmuir 20 (2004) 9821.
[12] D. Lu, G. Hitoki, E. Katou, J. Kondo, M. Hara, K. Domen, Chem. Mater. 16 (2004) 1603.
[13] T. Murase, H. Irie, K. Hashimoto, J. Phys. Chem. B 108 (2004) 15803.
[14] H. Fu, C. Pan, W. Yao, Y. Zhu, J. Phys. Chem. B 109 (2005) 22432.
[15] H. Fu, L. Zhang, W. Yao, Y. Zhu, Appl. Catal. B: Environ. 66 (2006) 100.
[16] R. Asahi, T. Morikawa, K. Aoki, Y. Taga, Science 293 (2001) 269.
[17] A. Kato, A. Kudo, J. Phys. Chem. B 105 (2001) 4285.
[18] T.J. Beck, A. Klust, M. Batzill, U. Diebold, C.D. Valentin, A. Selloni, Phys. Rev. Lett. 93 (2004) 1.
[19] W. Kohn, L.J. Sham, Phys. Rev. A 140 (1965) 1133.
[20] J.P. Perdew, Y. Wang, Phys. Rev. B 45 (1992) 13244.
[21] M.C. Payne, M.P. Teter, D.C. Allan, T.A. Arias, J.D. Joannopoulos, Rev. Mod. Phys. 64 (1992) 1045.
[22] R.M. Dreizler, E.K. Gross, Density Functional Theory: An Approach to the Quantum Many-Body Problem, Springer-Verlag, Berlin, 1990.